ACS APPLIED MATERIALS & INTERFACES

Letter

www.acsami.org

Robust Prototypical Anti-icing Coatings with a Self-lubricating Liquid Water Layer between Ice and Substrate

Jing Chen,[†,‡] Renmei Dou,[†,‡] Dapeng Cui,[†,‡] Qiaolan Zhang,[†,‡] Yifan Zhang,[†,‡] Fujian Xu,[§] Xin Zhou,[‡] Jianjun Wang,*[,†] Yanlin Song,[†] and Lei Jiang[†]

[†]Beijing National Laboratory for Molecular Sciences (BNLMS), Institute of Chemistry, Chinese Academy of Sciences, Beijing 100190, P. R. China

[‡]University of Chinese Academy of Sciences, Beijing 100190, P. R. China

[§]College of Materials Science & Engineering, Beijing University of Chemical Technology, Beijing 100029, P. R. China

Supporting Information

ABSTRACT: A robust prototypical anti-icing coating with a self-lubricating liquid water layer (SLWL) is fabricated via grafting cross-linked hygroscopic polymers inside the micropores of silicon wafer surfaces. The ice adhesion on the surface with SLWL is 1 order of magnitude lower than that on the superhydrophobic surfaces and the ice formed atop of it can be blown off by an action of strong breeze. The surface with self-lubricating liquid water layer exhibits excellent capability of self-healing and abrasion resistance. The SLWL surface should also find applications in antifogging and self-cleaning by rainfall, in addition to anti-icing and antifrosting.

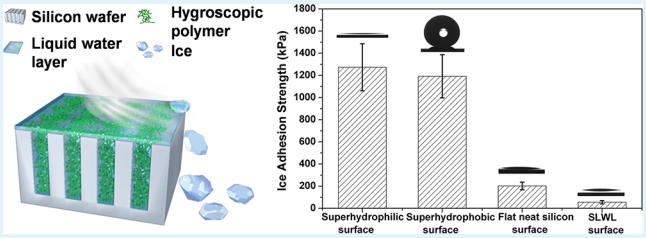

KEYWORDS: *anti-icing surface, hygroscopic polymer, ice adhesion, micropore arrayed silicon wafer, self-lubricating liquid water layer*

INTRODUCTION

Icing on exposed surfaces leads to operational difficulties and high maintenance efforts for power networks, aircrafts, ships, ground transportation vehicles, and house-hold refrigerators, to name but a few. In extreme cases, icing on surfaces causes disastrous events such as crash of aircrafts and collapse of power networks, which result in severe economic impact and large loss of life.[1−8] Over the last several decades, a large number of investigations have been carried out focusing on anti-icing surfaces,[9−20] but few surfaces have been found optimal for technological applications.[21−30] In real subfreezing environments, icing on surfaces occurs easily, for example the freezing rain drops freeze to form ice upon impact with any surfaces with temperature below 0 °C.[31,32] Therefore, ideal anti-icing surfaces should be that the ice adhesion on these surfaces is so small that ice formed on them can be shed off merely due to its own weight or a natural wind action. The adhesion strength between the skate blades and the ice decreases substantially due to the existence of a self-lubricating liquid water layer between the ice and the blades,[33] as such people can skate on the ice with grace and elegance. Inspired by ice skating, we report in this communication a robust prototypical anti-icing coating with a self-lubricating liquid water layer (SLWL) between the ice and the sample surface. The prototypical anti-icing coating shows a mechanical robustness to resist abrasion by a sandpaper and capability of self-healing.

RESULTS AND DISCUSSION

Figure 1a illustrates the fabrication of the robust prototypical anti-icing coating with a self-lubricating liquid water layer. A micropore arrayed silicon wafer surface is first prepared via a photolithographic process. Then cross-linked hygroscopic polymers synthesized by free radical polymerization are grafted inside the micropores. When the temperature is lowered, the hygroscopic polymer network inside micropores deliquesces and swells due to water absorption or condensation. If the temperature is sufficiently lowered and enough water is absorbed, the water swollen polymer network inside the micropores bulges out of micropores. The swollen polymers merge together due to molecular attractions between molecules, and a self-lubricating liquid water layer forms.[34] We want to point out here that the temperature range, where the self-lubricating liquid water layer exists, could be tuned by the water activity of the lubricating layer according to Koop et al.[35] One has to note that the inorganic material (here the silicon matrix for demonstration) endows the self-lubricating liquid water layer with a mechanical endurance and capability of self-healing, which are desired for technological applications. By introducing the self-lubricating liquid water layer between the ice and the sample surface, the ice adhesion on the sample surfaces is more than 1 order of magnitude lower than that on the superhydrophobic surfaces and the ice on this surface can

Received: March 23, 2013
Accepted: May 3, 2013
Published: May 3, 2013

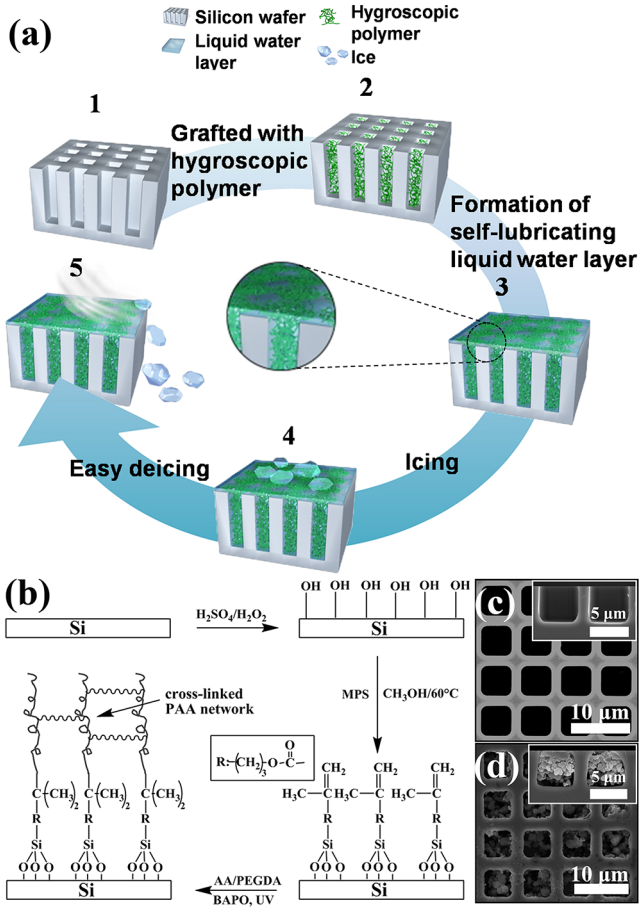

Figure 1. (a) Schematic illustration of the preparation of the self-lubricating liquid water layer surface. (1) Fabrication of micropore arrayed silicon wafer surfaces via a photolithographic process. (2) Grafting the micropore arrayed silicon wafer surfaces with cross-linked hygroscopic polymers. (3) Self-lubricating liquid water layer forms on micropore arrayed silicon wafer surfaces when condensation or deliquesce occurs. Inset is the magnified image of self-lubricating liquid water layer. (4) Ice formation atop of the self-lubricating liquid water layer. (5) Ice shed off with a wind action. (b) Preparation process of the micropore arrayed silicon wafer surface impregnated with cross-linked poly(acrylic acid) (PAA). Top view SEM images of representative micropore-arrayed silicon wafer surface (c) before and (d) after being grafted with crossed-linked hygroscopic polymers. Insets are the fracture-view SEM images of c and d.

be blown off with an action of strong breeze wind. Moreover the fabricated anti-icing surface exhibits an excellent capability of self-healing and abrasion resistance, on which the ice adhesion strength remains almost the same after several tens cycles of abrasion with a sandpaper. This work will certainly serve as a guideline for materials scientists to design organic/inorganic composite anti-icing coatings with an optimum performance.

Figure 1b shows the details of the grafting. After treated with a piranha solution (1:3 w/w H_2O_2/H_2SO_4), 3-(methacryloxypropyl)-trimethoxysilane (MPS) was attached on the hydroxylated silicon wafers.[36] Then the cross-linked poly(acrylic acid) (PAA) was grafted inside the silicon wafer by free radical polymerization.[37] Here we used water-soluble polyethylene glycol diacrylate (PEGDA) as the cross-linker. Figure 1c and Figure 1d show the scanning electron microscope (SEM) images of the representative micropore arrayed silicon wafer surface before and after grafting with the cross-linked hygroscopic polymer, where the pore is square column shaped with a side length of 5 μm and a depth of 5 μm and a spacing between two neighboring pores of 2 μm. Insets in panels c and d in Figure 1 are the fracture-view SEM images of a micropore arrayed silicon wafer surface before and after grafted with cross-linked hygroscopic polymers. The cross-linked hygroscopic polymer can be obviously observed inside the micropores after grafting. Furthermore, confocal microscopic images of representative micropore arrayed silicon wafer surface after grafting also demonstrate that the PAA was successfully grafted inside the pores (shown in Figure S1 in the Supporting Information).

Ice adhesion tested in a wind tunnel may mimic the environmental icing conditions. However, it is not practical for most academic laboratories because it requires a cold room and a complex system as well. Therefore we used another method to investigate the ice adhesion (see details in the Supporting Information). This method has been widely used in the literatures and gives a reproducible value of the ice adhesion on various surfaces, while the tests under freezing rain conditions (in a wind tunnel) are to be undertaken in the future. The variation of the ice adhesion strength with the area fraction, ϕ, is shown in Figure 2a ($\phi = a^2/(a + b)^2$, where a is the side

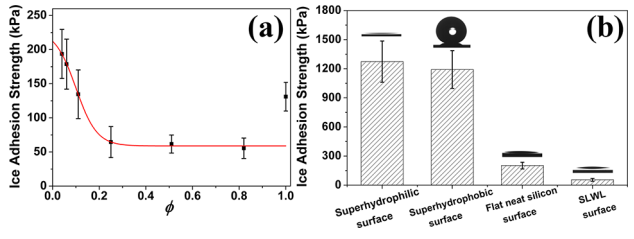

Figure 2. (a) Plots of the measured ice adhesion strength on the micropore arrayed silicon wafer surfaces impregnated with cross-linked hygroscopic polymers as a function of the area fraction, ϕ. The ice adhesion strengths on these surfaces were measured at −15 °C with a probe speed of 0.5 mm s^{-1}. (b) Average ice adhesion strengths on four different test surfaces. Insets are the profiles of water droplets on the corresponding surfaces.

length of the pore and b is the space between two neighboring pores). Ice adhesion on the self-lubricating liquid water layer surface decreased sharply as the ϕ value increased from 0 to 0.2, and then maintained a constant value (60 ± 16 kPa) when the ϕ is higher than 0.2. This can be rationalized by the formation of a continuous self-lubricating water layer. When ϕ is smaller than 0.2, the surface cannot be fully covered by the swollen polymer network. When the temperature is lowered below the freezing point, the liquid water on the uncovered surface freezes, as such a continuous self-lubricating liquid water layer cannot form between the ice and the sample surface, which leads to a sharply increased ice adhesion strength. This regime was defined as mixed lubrication by Hersey.[38] When the ϕ value is greater than 0.2, a continuous lubricating film forms between the ice and the sample surface, probably entering a regime of thick-film lubrication.[39] It is interesting to note that ice adhesion on an equivalent hydrogel grafted flat surface was 113 ± 21 kPa. It is understandable when one considers that ice adhesion on hydrogel grafted flat surface could be further varied by the thickness and viscosity of the hydrogel, which is currently under investigation.

dx.doi.org/10.1021/am401004t | ACS Appl. Mater. Interfaces 2013, 5, 4026−4030

Ice adhesion strength on the surface with a self-lubricating liquid water layer was further compared with other three surfaces (superhydrophilic, superhydrophobic and flat hydrophilic) with different chemical compositions and physical morphologies (Figure 2b). Superhydrophilic and superhydrophobic surfaces have the same morphology as the surface with the self-lubricating liquid water layer before grafting, i.e., they all consist of micropore array of 20 μm in width, 5 μm in depth and 2 μm in space between neighboring micropores (ϕ is 0.82, bigger than 0.2). Superhydrophilic and superhydrophobic surfaces were obtained by treating micropore arrayed silicon wafer surfaces with a piranha solution and (heptadecafluoro-1, 1, 2, 2-tetradecyl)-trimethoxysilane, respectively. Water contact angles (CA) on the superhydrophilic and superhydrophobic surface are 2.8 ± 0.5° and 152.0 ± 1.3°, respectively. The sliding angle for a 5 μL drop on the superhydrophobic surface was only 6.3°, indicating a low contact angle hysteresis on the superhydrophobic surface. Flat silicon wafer was treated by the piranha solution to have the flat neat hydrophilic surface (CA = 8.5 ± 1.2°). Surfaces with the self-lubricating liquid water layer (CA = 8.7 ± 1.4°) were fabricated by grafting the micropores with cross-linked poly(acrylic acid) as shown in Figure 1b. The insets of Figure 2b show the profiles of water droplets on the corresponding surfaces. The ice adhesion strengths on the superhydrophilic sufaces and superhydrophobic surfaces are almost the same, i.e., 1273 ± 212 and 1192 ± 195 kPa, respectively, which is six times as large as that on the flat neat hydrophilic silicon wafer surface, i.e., 202 ± 34 kPa. This could be explained when the mechanical interlocking between the ice and the surface textures of the superhydrophobic and superhydrophilic surfaces is considered. When the temperature is lowered, water molecules adsorb at the wall of the surface texture, which makes the surfaces more hydrophilic. At the same time, condensation occurs inside the surface texture. Then the liquid water is not at the Cassie state anymore, i.e., it penetrates partially or even completely into the surface texture.[40] We have measured the water contact angles on the surface at 25 °C (it is superhydrophobic at the room temperature), and found that the water contact angle decreased from 152.7° ± 1.0° at the room temperature to 126.3° ± 3.8° at the 2 °C, which clearly show that the liquid water drop is not at the Cassie state anymore. When the temperature is sufficiently lowered, partially or completely penetrated liquid water transforms to ice and the mechanical interlocking are formed between the ice and the surface texture, thus the ice adhesion increases greatly.[41] Therefore, the ice adhesion strengths on the superhydrophobic surface and superhydrophilic surface with the same physical morphology are almost the same.[29] The ice adhesion strength on the self-lubricating liquid water layer surfaces is the smallest, 55 ± 15 kPa, which is more than 20 times smaller than those on the superhydrophilic and superhydrophobic surfaces and is almost four times smaller than that on the flat neat hydrophilic silicon wafer surface. It is worthwhile to mention that the ice on the self-lubricating liquid water layer surface can be blown off with a wind speed of 12 m s^{-1}, whereas the ice on the other surfaces remains still as shown in Movie S1 in the Supporting Information. According to Beaufort's scale of wind force, this wind force is grade 6, the strong breeze.[42]

The existence of the self-lubricating liquid water layer is consolidated by investigating the temperature dependence of ice adhesion strength on this surface as shown in Figure 3. Ice adhesion strength on surfaces with self-lubricating liquid water

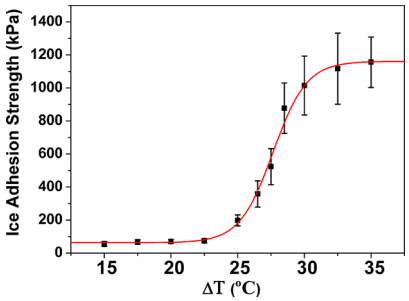

Figure 3. Ice adhesion strength on the self-lubricating liquid water layer surface versus the supercooling. The sharp increase of the ice adhesion at −25 °C signifies the disappearance of the self-lubricating liquid water layer due to the phase transition of the liquid water to the ice.

layer remained almost the same (67 ± 8 kPa) as the temperature was lowered till −25 °C. When the temperature was further decreased, the ice adhesion increased sharply and reached another value of 1156 ± 152 kPa around −30 °C. Below this temperature the ice adhesion strength remained constant again. The evolution of the value of the ice adhesion strength (τ) with the temperature (T) can be very well fitted with a sigmoid function (solid line) of the following form

$$\tau = 63 + 1099/(1 + \exp((T + 28)/1.26)) \quad (1)$$

sigmoid functions are quite common in the first order phase transition.[43] In our case the lower adhesion strength above −25 °C signifies the existence of the self-lubricating liquid water layer. The sharp increase of the ice adhesion strength represents the onset of the mechanical interlocking between the ice and the surface texture as a result of the phase transition of the liquid water to the ice. According the fitting equation, the phase transition temperature is −28 °C, which could be further lowered if the type and concentration of hygroscopic polymer networks in the micropores varied. For example, the phase transition temperature was as low as −60 °C for the polyacrylamide gel with 30% (w/w).[44] In the case of polyvinyl alcohol (PVA), the water could be kept liquid even at −100 °C when the PVA concentration reaches 80% (w/w).[45]

The durability of anti-icing performance of the SLWL surface was studied via icing/deicing as shown in Figure S2 in the Supporting Information. Ice adhesion strengths on SLWL surfaces are nearly constant after the icing/deicing test. We further investigated the capability of abrasion resistance and self-healing of the anti-icing surface with a homemade setup, where a sandpaper (10 000 mesh) was used as an abrasion media (see Figure S3 in the Supporting Information). The silicon wafer was glued to a 500 g weight with the self-lubricating liquid water layer in close contact with the sandpaper. The gravity of the weight can be transferred to a pressure of 12.5 kPa, with which the sandpaper applied to the self-lubricating liquid water layer surface. The weight together with the silicon wafer was then dragged back and forth against the sandpaper with a speed and length of 0.5 mm s^{-1} and 10 mm, respectively (one back and forth cycle with a distance of 10 mm represents one abrasion cycle).

Figure 4 shows the evolution of the ice adhesion strength with the abrasion cycle. Although the average surface roughness of the area between the pores on the silicon wafer surface changed greatly from 9.48 nm (Figure 4a) to 72.47 nm (Figure 4b) and the depth of hole was reduced from 5 μm to 1.38 ±

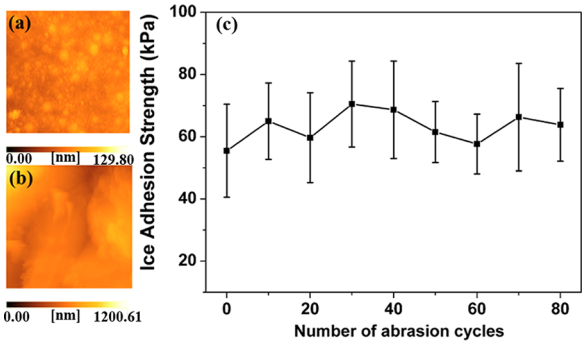

Figure 4. Atomic force microscopy (AFM) images (2 μm × 2 μm) of the area between pores on the SLWL surface (a) before and (b) after abrasion. The average surface roughness (R_a) at the area between pores was increased greatly, increased from 9.48 nm before the abrasion to 72.47 nm after abrasion. (c) Average ice adhesion strengths on the anti-icing surface with self-lubricating liquid water layer remained almost the same after several tens cycles of abrasion test with a normal loading of 12.5 kPa by a 10 000 mesh sandpaper, which clearly shows that the fabricated anti-icing surface have the capability of self-healing and abrasion resistance.

1.02 μm, the ice adhesion strength on the self-lubricating liquid water layer surface maintained almost the same even after 80 cycles of abrasion, 63 ± 11 kPa. This can be rationalized by the self-healing capability of the self-lubricating liquid water layer. When the surface was abraded with the sandpaper, only the top surface of the pore is in close contact with the sandpaper. The hygroscopic polymer network inside the micropores was protected from being removed during the abrasion. The self-lubricating liquid water layer forms and covers the roughened surface when the polymer network deliquesces, swells and finally merges under the action of the capillary force.[34]

It is interesting to note that Wong and co-workers recently reported slippery liquid-infused porous surfaces (SLIPS) as omniphobic surfaces, which was inspired by the surface of the insect-eating *pitcher plant Nepenthes*.[46] These surfaces repel pure liquids (water, oil), complex liquids (crude oil, blood), ice and even to insects. Moreover SLIPS integrate the capabilities of self-lubricating, self-healing and self-cleaning. The SLIPS are not only of fundamental interest but also have promising applications. However, the SLIPS are compromised by the strict restrictions on the infused liquids, i.e., the porous substrates must be wetted preferentially by the infused liquid and at the same time the infused liquid must be immiscible with the water and oils.[47] Moreover, the durability of the SLIPS is limited by the evaporation of the perfluorinted liquids.[48] In our work, a layer of liquid water was introduced between the ice and the substrate, which is certainly eco-friendly and does no harm to the environment. Furthermore, whenever ice or frost is placed atop of the coating, the part of the ice or frost in contact with the fabricated surface melts and forms a self-lubricating liquid water layer. As such, our anti-icing surface should have long durability and it is viable in both low and high humidity environments. It is worth to mention that the rim of Nepenthes pitcher plants is slippery because of condensation of water on the hygroscopic nectar at the peristome surface, which causes insects to fall into the trap.[49]

CONCLUSION

In conclusion, we have fabricated a robust prototypical anti-icing coating with a self-lubricating liquid water layer between the ice and the sample surface via grafting cross-linked hygroscopic polymers inside the micropores at the surface of inorganic materials. The ice adhesion strength on the surface with self-lubricating liquid water layer is 1 order of magnitude lower than that on superhydrophilic or superhydrophobic surfaces. The accumulated ice on the surface with a self-lubricating liquid water layer can be blown off by an action of strong breeze. Moreover, the self-lubricating liquid water layer surface exhibits excellent mechanical endurance and capability of self-healing. The self-lubricating liquid water layer coatings should also find applications in antifogging and self-cleaning by rainfall, in addition to anti-icing and antifrosting.

ASSOCIATED CONTENT

Supporting Information

Experimental details including sample preparation, instrumentation, and experimental results, as well as additional information as noted in text. This material is available free of charge via the Internet at http://pubs.acs.org.

AUTHOR INFORMATION

Corresponding Author

*E-mail: wangj220@iccas.ac.cn.

Notes

The authors declare no competing financial interest.

ACKNOWLEDGMENTS

JW acknowledges sincerely the beneficial discussion with Prof. Dr. G. Wegner. The authors are grateful for the financial support from the Chinese National Nature Science Foundation (Grants 51173196, 21004068, 21121001), and the 973 Program (2012CB933800, 2013CB933004).

REFERENCES

(1) Yao, X.; Song, Y.; Jiang, L. *Adv. Mater.* **2011**, *23*, 719−734.
(2) Xiao, J.; Chaudhuri, S. *Langmuir* **2012**, *28*, 4434−4446.
(3) Jung, S.; Tiwari, M. K.; Doan, N. V.; Poulikakos, D. *Nat. Commun.* **2012**, *3*, 615.
(4) Petrie, E. M. *Metal Finishing* **2009**, *107*, 56−59.
(5) Kasaai, M. R.; Farzaneh, M. *Proceedings of OMAE04: 23rd International Conference on Offshore Mechanics and Arctic Engineering*; Vancouver, British Columbia, Canada, June 20−25, 2004 ; American Society of Mechanical Engineers (ASME): New York, 2004; pp 927−932.
(6) Porte, H. A.; Nappier, T. E. *Coating Materials for Prevention of Ice and Snow Accumulations−A Literature Survey*; U.S. Naval Engineering Laboratory Report TN-541 ; U.S. Naval Civil Engineering Laboratory: Port Hueneme, CANovember 12, 1963.
(7) Sayward, J. M. *Seeking Low Ice Adhesion, Special Report 79−11*; U.S. Army Cold Regions Research and Engineering Laboratory:Hanover, NH, 1979.
(8) Farzaneh, M. *Atmospheric Icing of Power Networks*; Springer: New York, 2008, pp. 327−369.
(9) Mishchenko, L.; Hatton, B.; Bahadur, V.; Taylor, A. J.; Krupenkin, T.; Aizenberg, J. *ACS Nano* **2010**, *4*, 7699−7707.
(10) Tourkine, P.; Merrer, M. Le; Quéré, D. *Langmuir* **2009**, *25*, 7214−7216.
(11) Guo, P.; Zheng, Y.; Wen, M.; Song, C.; Lin, Y.; Jiang, L. *Adv. Mater.* **2012**, *24*, 2642−2648.
(12) Wang, F.; Li, C.; Lv, Y.; Lv, F.; Du, Y. *Cold Reg. Sci. Technol.* **2010**, *62*, 29−33.
(13) Boinovich, L. B.; Emelyanenko, A. M. *Mendeleev Commun.* **2013**, *23*, 3−10.
(14) Boinovich, L. B.; Emelyanenko, A. M.; Ivanov, V. K.; Pashinin, A. S. *ACS Appl. Mater. Interfaces* **2013**, *5*, 2549−2554.

(15) McKiney, G. H.; Meuler, A. J.; Smith, J. D.; Varanasi, K. K.; Mabry, J. M.; Cohen, R. E. *ACS Appl. Mater. Interfaces* **2010**, *2*, 3100−3110.
(16) Kulinich, S. A.; Farzaneh, M. *Langmuir* **2009**, *25*, 8854−8856.
(17) Kulinich, S. A.; Farzaneh, M. *Cold Reg. Sci. Technol.* **2011**, *65*, 60−64.
(18) Antonini, C.; Innocenti, M.; Horn, T.; Marengo, M.; Amirfazli, A. *Cold Reg. Sci. Technol.* **2011**, *67*, 58−67.
(19) Cao, L.; Jones, A. K.; Sikka, V. K.; Wu, J.; Gao, D. *Langmuir* **2009**, *25*, 12444−12448.
(20) He, M.; Wang, J.; Li, H.; Song, Y. *Soft Matter* **2011**, *7*, 3993−4000.
(21) Jung, S.; Dorrestijn, M.; Raps, D.; Das, A.; Megaridis, C. M.; Poulikakos, D. *Langmuir* **2011**, *27*, 3059−3066.
(22) Li, K.; Xu, S.; Shi, W.; He, M.; Li, H.; Li, S.; Zhou, X.; Wang, J.; Song, Y. *Langmuir* **2012**, *28*, 10749−10754.
(23) He, M.; Wang, J.; Li, H.; Jin, X.; Wang, J.; Liu, B.; Song, Y. *Soft Matter* **2010**, *6*, 2396−2399.
(24) Li, Y.; Li, L.; Sun, J. *Angew. Chem., Int. Ed.* **2010**, *49*, 6129−6133.
(25) Nosonovsky, M.; Hejazi, V. *ACS Nano* **2012**, *6*, 8488−8491.
(26) He, M.; Li, H.; Wang, J.; Song, Y. *Appl. Phys. Lett.* **2011**, *98*, 093118.
(27) Farhadi, S.; Farzaneh, M.; Kulinich, S. A. *Appl. Surf. Sci.* **2011**, *257*, 6264−6269.
(28) Jafari, R.; Menini, R.; Farzaneh, M. *Appl. Surf. Sci.* **2010**, *257*, 1540−1543.
(29) Chen, J.; Liu, J.; He, M.; Li, K.; Cui, D.; Zhang, Q.; Zeng, X.; Zhang, Y.; Wang, J.; Song, Y. *Appl. Phys. Lett.* **2012**, *101*, 111603.
(30) Kim, P.; Wong, T.-S.; Alvarenga, J.; Kreder, M. J.; Adorno-Martinez, W. E.; Aizenberg, J. *ACS Nano* **2012**, *6*, 6569−6577.
(31) Varanasi, K. K.; Deng, T.; Smith, J. D.; Hsu, M.; Bhate, N. *Appl. Phys. Lett.* **2010**, *97*, 234102.
(32) Alizadeh, A.; Bahadur, V.; Zhong, S.; Shang, W.; Li, R.; Ruud, J.; Yamada, M.; Ge, L.; Dhinojwala, A.; Sohal, M. *Appl. Phys. Lett.* **2012**, *100*, 111601.
(33) Rosenberg, R. *Phys. Today* **2005**, *58*, 50−55.
(34) Ishino, C.; Reyssat, M.; Reyssat, E.; Okumura, K.; Quéré, D. *Europhys. Lett.* **2007**, *79*, 56005.
(35) Koop, T.; Luo, B.; Tsias, A.; Peter, T. *Nature* **2000**, *406*, 611−614.
(36) Demirel, G. B.; Çaykara, T. *Appl. Surf. Sci.* **2009**, *255*, 6571−6576.
(37) Diao, Y.; Harada, T.; Myerson, A. S.; Alan Hatton, T.; Trout, B. L. *Nat. Mater.* **2011**, *10*, 867−871.
(38) Hersey, M. D.; *Theory and Research in Lubrication*; Wiley: New York, 1966.
(39) Szeir, A. Z. *Fluid Film Lubrication Theory and Design*; Cambridge University Press: Cambridge, U.K., 2005; Chapter 1, pp 30−32.
(40) Karmouch, R.; Ross, G. G. *J. Phys. Chem. C* **2010**, *114*, 4063−4066.
(41) Kulinich, S. A.; Farhadi, S.; Nose, K.; Du, X. W. *Langmuir* **2011**, *27*, 25−29.
(42) Soligo, M. J.; Irwin, P. A.; Williams, C. J.; Schuyler, G. D. *J. Wind Eng. Ind. Aerod.* **1998**, *77&78*, 753−766.
(43) Tobin, M. C. *J. Polym. Sci., Polym. Phys.* **1976**, *14*, 2253−2257.
(44) Katayama, S.; Fujiwara, S. *J. Phys. Chem.* **1980**, *84*, 2320−2325.
(45) Ping, Z. H.; Nguyen, Q. T.; Chen, S. M.; Zhou, J. Q.; Ding, Y. D. *Polymer* **2001**, *42*, 8461−8467.
(46) Wong, T.-S.; Kang, S. H.; Tang, S. K. Y.; Smythe, E. J.; Hatton, B. D.; Grinthal, A.; Aizenberg, J. *Nature* **2011**, *477*, 443−447.
(47) Stone, H. A. *ACS Nano* **2012**, *6*, 6536−6540.
(48) Nosonovsky, M. *Nature* **2011**, *477*, 412−413.
(49) Bohn, H. F.; Federle, W. *Proc. Natl. Acad. Sci. U.S.A.* **2004**, *101*, 14138−14143.